Compensatory Drift and the Evolutionary Dynamics of Dosage-Sensitive Duplicate Genes

Ammon Thompson,*,†,1,2 Harold H. Zakon,*,† and Mark Kirkpatrick*
*Department of Integrative Biology and †Department of Neuroscience, University of Texas, Austin, Texas 78712

ABSTRACT Dosage-balance selection preserves functionally redundant duplicates (paralogs) at the optimum for their combined expression. Here we present a model of the dynamics of duplicate genes coevolving under dosage-balance selection. We call this the *compensatory drift model*. Results show that even when strong dosage-balance selection constrains total expression to the optimum, expression of each duplicate can diverge by drift from its original level. The rate of divergence slows as the strength of stabilizing selection, the size of the mutation effect, and/or the size of the population increases. We show that dosage-balance selection impedes neofunctionalization early after duplication but can later facilitate it. We fit this model to data from sodium channel duplicates in 10 families of teleost fish; these include two convergent lineages of electric fish in which one of the duplicates neofunctionalized. Using the model, we estimated the strength of dosage-balance selection for these genes. The results indicate that functionally redundant paralogs still may undergo radical functional changes after a prolonged period of compensatory drift.

KEYWORDS duplication; expression evolution; dosage balance; neofunctionalization; whole-genome duplication

THE fate of duplicate genes is characterized by two extremes: degeneration and the origin of biological novelty. Early models for the evolutionary dynamics of duplicates suggested that typically one member of a duplicate pair would quickly degenerate into a nonfunctional pseudogene (Haldane 1933; Ohno 1970). More rarely, a duplicate instead may evolve a novel function in a process called *neofunctionalization* (Muller 1936; Ohno 1970; Ohta 1987). The time scale for either pseudogenization or neofunctionalization is expected to be on the order of a few million years (Lynch and Conery 2000).

Recent research indicates, however, that the evolutionary dynamics for many duplicates are not so simple (Walsh 1995, 2003; Force *et al.* 1999; Papp *et al.* 2003; He and Zhang 2005; Rastogi and Liberles 2005; Scannell and Wolfe 2008; Qian *et al.* 2010; Kondrashov 2012). Some genes are *dosage sensitive*, meaning that a change in their copy number alters expression and disrupts the stoichiometric balance of their gene products with those of other genes. Duplicates of dosage-sensitive genes typically will fix in a population only if they originate in a whole-genome duplication (WGD), where all interacting partners duplicate together. Selection to maintain the stoichiometric relations between the products of duplicate genes, termed *dosage-balance selection*, can preserve duplicates as functionally redundant copies for prolonged periods of time (Birchler *et al.* 2001, 2005; Veitia 2002; Papp *et al.* 2003; Aury *et al.* 2006; Blomme *et al.* 2006; Freeling and Thomas 2006; Stranger *et al.* 2007; Qian and Zhang 2008; Edger and Pires 2009; Makino and McLysaght 2010; Konrad *et al.* 2011; Birchler and Veitia 2012; McGrath *et al.* 2014a).

Recent data on a pair of sodium channel duplicates in teleost fish are consistent with the expectations of the dosage-balance hypothesis (Thompson *et al.* 2014). The two duplicates, also called *paralogs*, have been conserved in muscle cells for over 300 million years since the teleost-specific WGD. In two independent lineages of electric fish, however, only one of the sodium channels is expressed in muscle cells. The other duplicate neofunctionalized and now plays a key role in the electric organ (Novak *et al.* 2006; Zakon *et al.* 2006; Arnegard *et al.* 2010). These convergent neofunctionalization events happened on a very slow time scale, more than 100 million years after duplication (Arnegard *et al.* 2010; Lavoué *et al.* 2012; Betancur-R *et al.* 2013). The phylogenetic context for the evolution of the duplicates is shown in Figure 1.

doi: 10.1534/genetics.115.178137
Manuscript received May 13, 2015; accepted for publication December 6, 2015; published Early Online December 9, 2015.
Supporting information is available online at www.genetics.org/lookup/suppl/doi:10.1534/genetics.115.178137/-/DC1
[1]Present address: Department of Evolution and Ecology, University of California, Davis, One Shields Avenue, Davis, CA 95616.
[2]Corresponding author: Department of Evolution and Ecology, University of California, Davis, CA 95616. E-mail: ammthompson@ucdavis.edu

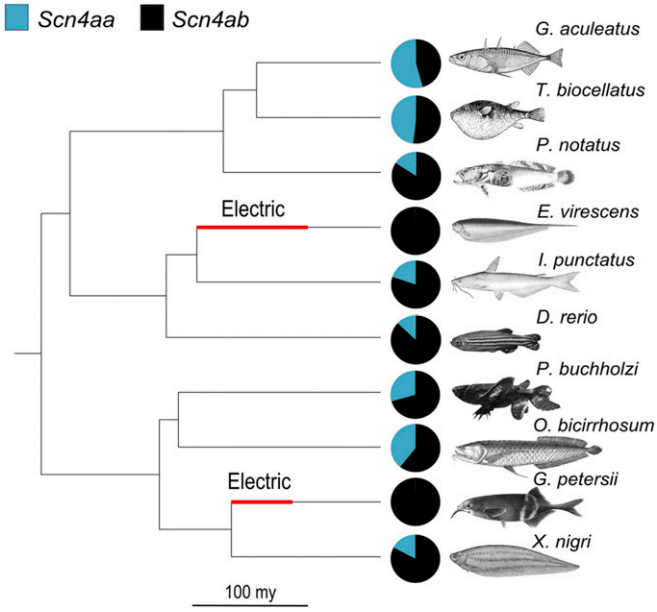

Figure 1 Sodium channel expression and phylogenetic relationships of 10 teleost fish species. The families represented here span almost the entire teleost clade. The relative expression in skeletal muscle of the voltage-gated sodium channel genes *Scn4aa* and *Scn4ab* is represented with pie charts for each of the 10 species. Thick red segments on the branches leading to the two electric fish *Eigenmannia veriscens* and *Gnathonemus petersii* indicate the likely times when electric organs evolved and *Scn4aa* neofunctionalized (Arnegard *et al.* 2010; Betancur-R *et al.* 2013).

Thompson *et al.* (2014) proposed that in the teleost ancestor the duplicates were preserved after WGD by dosage-balance selection. They hypothesized that under this selective constraint, one paralog gradually drifted to lower expression levels, while the other compensated by evolving higher expression. Eventually, one paralog contributed so little to its original function that it could be neofunctionalized in the electric organ without major compromise to muscles. This mode of evolution also may explain comparative expression patterns observed in some ciliates (Gout and Lynch 2015) as well as some mammals (Lan and Pritchard 2015). This hypothesis raises theoretical and quantitative issues not previously explored. Can dosage-balance selection in fact maintain duplicates for hundreds of millions of years? Will this mode of evolution produce comparative patterns in a phylogeny that are distinct from other models? And how does this evolutionary process affect the likelihood of neofunctionalization?

Here we develop a model for the evolution of paralog expression under dosage-balance selection. It envisions a process, which we call *compensatory drift*, in which paralogs diverge by weakly selected mutations that fix largely by drift. The model shows how key genetic parameters determine the time scale over which duplicates are maintained before one is lost or neofunctionalizes. The evolutionary dynamics are determined by just two compound parameters. The first is a speed parameter that relates mutation, selection, and random genetic drift to the rate at which the duplicates' expression diverges. The second is a threshold parameter that determines the point at which expression of one duplicate is sufficiently low that it is largely relieved from dosage-balance constraints and free to evolve a novel function. The model predicts two phases of evolution. In the initial phase, the difference in expression between functionally identical paralogs drifts randomly while their combined expression remains nearly constant. In the second phase, the expression threshold is reached, and one of the duplicates quickly accrues function-altering substitutions.

We fit the compensatory drift model to data from Thompson *et al.* (2014) on the expression of sodium channel duplicates in 10 families of teleost fish. Our estimate for the speed parameter is consistent with what is known about the biological parameters that feed into it, suggesting that compensatory drift is a plausible model for sodium channel evolution. Our estimate for the threshold parameter is, to our knowledge, the first available. Finally, we demonstrate that dosage-balance selection can greatly enhance the probability of neofunctionalization compared to the classic neutral scenario. These results suggest that WGD, as well as contexts in which dosage-balance selection acts, may be a particularly rich source of genetic novelty for geologically long periods of time.

Materials and Methods

The model

After duplication, stabilizing selection favors an optimal total expression of two paralogs. A mutation that affects expression of either one will either increase or decrease fitness depending on whether it brings total expression closer to or further from the optimum. Mutations also experience random genetic drift, so there is a nonzero probability that both mildly deleterious and beneficial mutations will be established.

We visualize compensatory drift as a series of fixation events that change the expression of the duplicates. A schematic of the process is shown in Figure 2. The two paralogs evolve in an anticorrelated pattern. Mutations in one duplicate can move the total expression away from its optimum. Compensatory mutations in the other duplicate tend to move total expression closer to the optimum. The result is that total expression remains close to the optimum, while the difference in their expression fluctuates randomly. The state of the population at any time is described by the total expression of the two duplicates and the difference in expression between them. If expression evolves to a point at which one of the duplicates produces the bulk of the gene product, selection is no longer strong enough to prevent function-altering substitutions from accruing in the paralog with lower expression. This threshold can be interpreted as either the point where pseudogenization quickly occurs or where the benefit of neofunctionalization outweighs the fitness tradeoff from loss of the ancestral function.

Assumptions

The expression levels of two duplicates are denoted as p_1 and p_2. We assume that stabilizing selection acts on the sum of

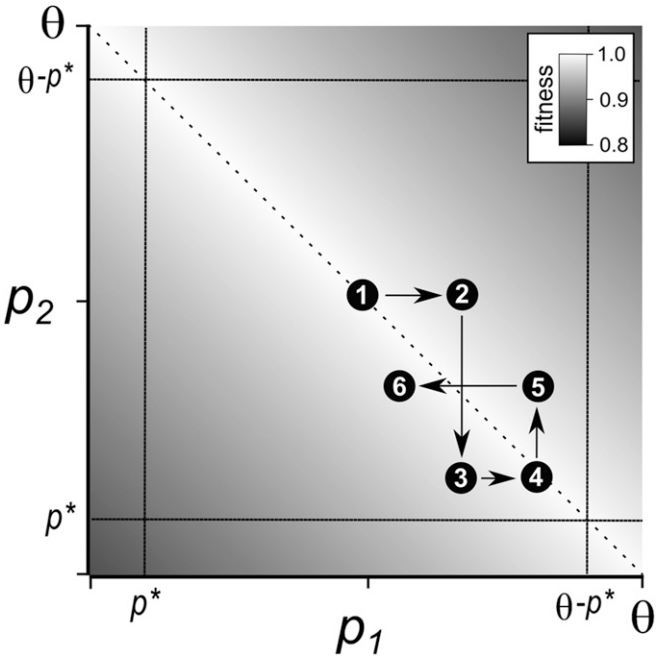

Figure 2 Schematic of the coevolution of paralog expression under compensatory drift. Axes show the expression of the duplicate genes, and fitness is represented with a gray scale. The dashed diagonal line shows the maximal fitness where $p_1 + p_2 = \theta$. The dotted vertical and horizontal lines show the expression thresholds where a duplicate loses its original function. A sequence of several consecutive expression changes is shown with numbered circles.

expression $A = p_1 + p_2$. The fitness function acting on A is proportional to a normal distribution with mean equal to the optimum for total expression θ and with variance ω^2 (which are assumed to be constant in time). The variance parameter determines the strength of selection, where larger values of ω^2 indicate weaker stabilizing selection. No selection acts on the difference in expression $D = p_1 - p_2$.

Mutations occur in the regulatory regions of each of the four gene copies at a rate μ per generation. They evolve according to a Fisher-Wright model of drift and selection. Mutations enter the population at a rate of $4N\mu$, where N is the population size. Their effects on expression are additive. The effect of a given mutation on p_1 or p_2, which we denote as δ, is normally distributed with mean 0 and variance σ_m^2. We therefore assume that the distribution of mutational effects is constant in time and independent of a gene's current level of expression. Biologically, this means that the regulation of expression is free of complicated forms of epistasis.

New mutations are either lost or fixed under the combined forces of selection and drift. We assume that mutation is weak ($4N\mu \ll 1$), so there is a negligible chance that more than one mutation will be segregating. (We will return to this point in the *Results* section, which suggests that the model also may be a good approximation when that assumption is violated.) Evolution thus proceeds by a series of fixation events at the two loci. This is a Poisson process, and the waiting time between mutations is exponentially distributed with mean of $1/(4N\mu)$ generations.

We calculate the fixation probability for each mutation using the diffusion approximation of Kimura (1962)

$$P_{\text{fix}} = \frac{1 - e^{-2s}}{1 - e^{-4Ns}} \tag{1}$$

where s is the selection coefficient of the new mutation

$$s \approx -\frac{\delta^2}{2\omega^2} \tag{2}$$

Equation 2 is an approximation that neglects the deviation of the population from the optimum θ. The approximation is valid when the SD of mutational effects is large relative to the typical deviation from the optimum. We verified the accuracy of the approximation using parameter values consistent with the data on teleost sodium channels from Thompson *et al.* (2014) (Supporting Information, File S1).

We assume that when the duplication occurs, the two paralogs have equal expression, and their total expression is optimal ($D = 0$ and $A = \theta$). As evolution proceeds, expression of the duplicates eventually will fall to a threshold level, denoted p^*, while its paralog rises to $\theta - p^*$. At this point, the paralog with lower expression rapidly either becomes a pseudogene or neofunctionalizes. This threshold is represented in our model by a critical difference in the expression of the duplicates $D^* = \theta - 2p^*$. If D reaches either D^* or $-D^*$, then one or the other duplicate loses its original function.

Evolutionary dynamics

Our goal is to determine the probability distribution for expression levels at times following the duplication event. Simulations reveal that under plausible parameter values, evolutionary trajectories are confined to values of A that are very close to θ (File S1). This suggests that the dynamics can be approximated by a one-dimensional diffusion in the expression difference $D = p_1 - p_2$. We write the probability density of D at time t following the duplication as $F(D, t)$. The evolution of the density function is described by

$$\frac{\partial}{\partial t}F(D,t) = \frac{1}{2}\sigma_D^2\frac{\partial^2}{\partial D^2}F(D,t) \tag{3}$$

This is the heat equation (Cox and Miller 1965), where σ_D^2 is the diffusion parameter. This parameter determines the speed at which D evolves, and it equals the rate of increase in variance of the probability distribution D per generation. File S2 shows that

$$\sigma_D^2 = k\frac{\mu\omega^3}{\sigma_m N^{3/2}} \tag{4}$$

where k is a constant that is independent of the model's parameters. It is difficult to calculate analytically, so we determined its value ($k \approx 1.543$) numerically (File S2).

From Equation 4, we gain insight into the impact of biological parameters on the speed at which D evolves. Imagine that we follow a set of evolutionary lineages that began to

diverge independently after the duplication event. The variance in the distribution of D initially increases at a constant rate and is equal to $\sigma_D^2 t$ at t generations after duplication. Thus, the diffusion rate σ_D^2 sets the speed of divergence, as illustrated in Figure 3. Equation 4 shows how the biological parameters affect this speed. The speed is reduced by larger population sizes. Larger values of N cause a greater number of mutations to enter the population in each generation but also increase the efficiency of purifying selection; the net result is that a smaller number of mutations fix (see Equation 1). Equation 4 also shows that the speed of divergence increases with higher mutation rates (larger μ) and decreased strengths of selection (larger ω^2). A somewhat counterintuitive result is that the speed of divergence declines as the average effect size of mutations σ_m increases. This is so because larger mutations are more likely to be strongly deleterious and therefore very unlikely to fix.

To summarize the model, the probability density of D evolves according to Equation 3, with initial condition $D = 0$ at $t = 0$ and with absorbing barriers at $\pm D^*$. Before doing any further analysis, Equation 3 tells us a simple but important fact: although the model is based on six underlying biological parameters (μ, ω, σ_m, N, θ, and p^*), the evolutionary dynamics are governed by only two: the speed parameter σ_D^2 and the threshold D^*.

The solution for the density function of D is

$$F(D,t) = \frac{1}{\sqrt{2\pi\sigma_D^2 t}} \sum_{n=-\infty}^{\infty} \left\{ \exp\left(-\frac{(D+4nD^*)^2}{2\sigma_D^2 t}\right) - \exp\left(-\frac{(D+(4n-2)D^*)^2}{2\sigma_D^2 t}\right) \right\} \quad (5)$$

for $-D^* < D < D^*$ (Cox and Miller 1965). The probability that one of the duplicates has either been lost as a pseudogene or has neofunctionalized after t generations is

$$P_{\text{loss}}(t) = 1 - \int_{-D^*}^{D^*} F(D,t)\,dD = 4\sum_{n=0}^{\infty} \left\{ \Phi\left(\frac{(4n+3)D^*}{\sqrt{\sigma_D^2 t}}\right) - \Phi\left(\frac{(4n+1)D^*}{\sqrt{\sigma_D^2 t}}\right) \right\} \quad (6)$$

where Φ denotes the standard normal cumulative distribution function (Cox and Miller 1965).

With Equation 6, we can infer how varying the biological parameters in Equation 4 affect the expected life span of duplicate genes. Figure 4 shows the result of varying each biological parameter of the model on the time scale of duplicate loss. These results imply that the time between duplication and loss can be very long, especially for large populations, genes under strong dosage constraints (small ω), and genes with high expression (large D^*). To get some idea of the time scale, we can calculate the number of generations needed to reach a probability of 1/2 that one of the duplicates is lost using parameter values that are plausible for the electric fish clades: a population size $N = 10^4$ and a mutation rate $\mu = 10^{-5}$. The strength of stabilizing selection ($\omega^2 = 81\ \sigma_m^2$) is such that 90% of mutations are strongly deleterious ($|Ns| > 1$) and so have negligible chance of fixation. The threshold is $D^* = 5\sigma_m$, which means that following duplication, the threshold p^* could in principle be reached with the fixation of just five mutations of typical size. (As we will see, however, this does not happen because most mutations are eliminated by dosage-balance selection.) Under these assumptions, we find from Equation 6 that after 1.7 billion generations, there is still a 50% probability that neither gene will have been lost. Thus, dosage-balance selection can maintain functional paralogs for very long evolutionary periods. If we decrease the strength of dosage-balance selection such that half the mutations are nearly neutral ($\omega^2 = 2.3 \times 10^3 \sigma_m^2$), the amount of time decreases dramatically to just 11 million generations.

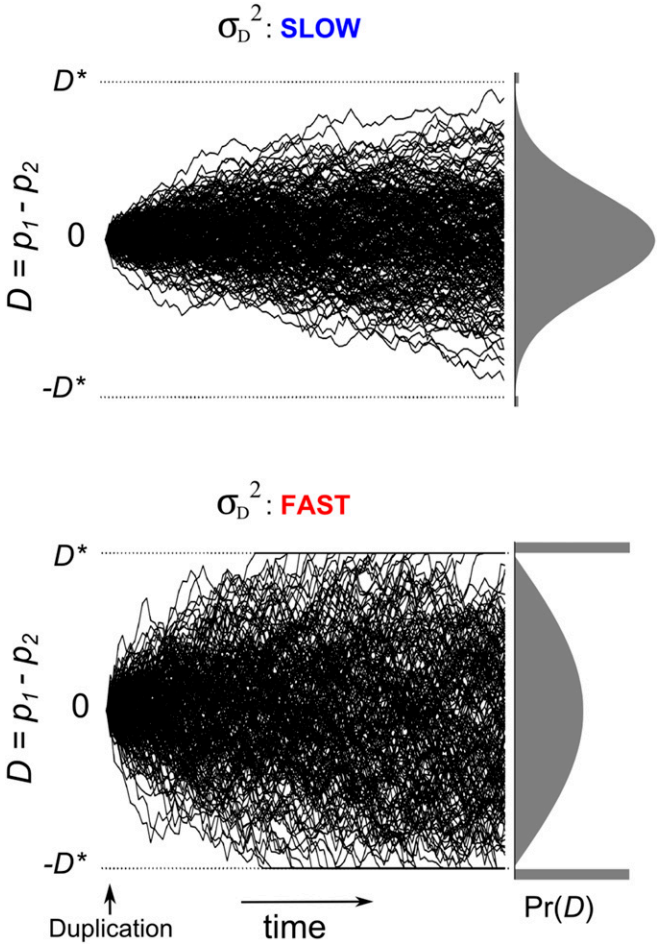

Figure 3 The speed of divergence in the expression of duplicate genes. Examples of the evolution of expression difference D (= $p_1 - p_2$) when the diffusion parameter σ_D^2 is small (top) and large (bottom). Each panel shows sample trajectories and the final probability distribution for D (at right). In the top panel, the final distribution of D is approximately normal; neofunctionalization and pseudogenization are rare. In the bottom panel, neofunctionalization is frequent (large rectangles outside the thresholds at $\pm D^*$).

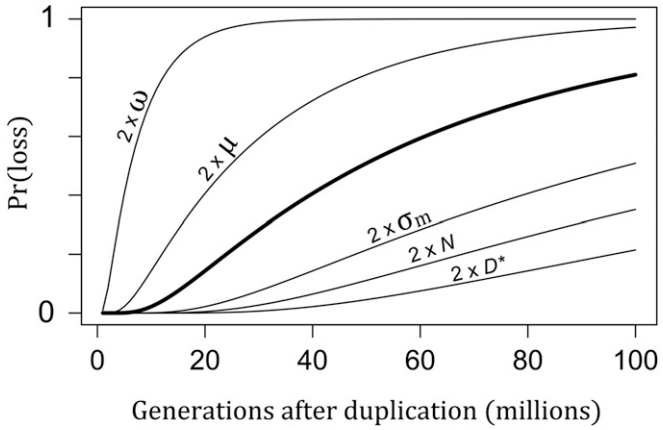

Figure 4 The probability of gene loss after duplication. The thick curve shows the probability of loss, either through pseudogenization or neofunctionalization, over time with standard parameter values: the selection strength is $\omega^2 = 10^4$, the SD of the mutation effect size is $\sigma_m = 1$, the population size is $N = 10^4$, the mutation rate is $\mu = 10^{-5}$, and the expression threshold is $D^* = 100$. Other curves show results when individual parameter values are doubled.

Data availability

Simulation code is available upon request.

Results

Fitting the model to data

To assess the plausibility of this model and to estimate parameters of biological interest, we fit this model to data on the expression of sodium channel duplicates from Thompson *et al.* (2014). The data are the relative expression levels of the two teleost-specific paralogs in 10 families of fish sampled broadly across the entire teleost clade and the phylogenetic relations between those families (Figure 1). The parameters being fit are the diffusion rate σ_D^2 and the threshold for gene loss D^*.

We used approximate Bayesian computation (ABC) because it allows inferences about models that are too complicated for statistical frameworks such as likelihood (Tavare *et al.* 1997; Beaumont *et al.* 2002; Beaumont 2010). The basic approach is to compare summary statistics measured from simulated data to the same statistics measured from real data. Estimates for the parameters are given by the values that produce simulated data sets that are most similar to the real data. In practice, this is accomplished by choosing values for the model parameters from prior distributions, simulating data using the model with those values, and comparing the summary statistics that result with those from the real data. The parameter values used in the simulation are rejected from the posterior distribution if the summary statistics from the real and simulated data sets are not sufficiently similar.

We simulated the evolution of expression on the phylogeny under the model described earlier. The output of the simulation gave the identities of the lineages (if any) that lost one of the paralogs to muscle function and the relative expression of the two paralogs for those lineages that have not. These results were compared to the actual data using two types of summary statistics. The first, which is binary, is determined by whether neofunctionalization occurred in the same locations on the tree as observed in the data. We rejected all simulations in which this pattern was not observed. The second kind of summary statistic was the independent contrasts (Felsenstein 1985) at the nodes of the phylogeny for the relative expression of the duplicates in the nonelectric fish. We rejected simulations if the Euclidean distance of the independent contrasts between the real and simulated data exceeded a threshold. Further details are given in File S3.

Including the electric fish data in the analysis upwardly biases our estimate of the probability of neofunctionalization. (The families of fish in the data set are not randomly chosen: it intentionally includes the only two families in which neofunctionalization is known.) To address this issue, we performed ABC analysis both with the electric fish and without them. Excluding the electric fish biases the estimate in the opposite direction, and therefore, the two analyses give boundaries for our estimates of model parameters.

The joint posterior distributions for the diffusion rate σ_D^2 and the threshold for gene loss D^* from the two analyses are shown in Figure 5. The distributions are quite similar. On a log-log plot, the values of $\log\sigma_D^2$ and $\log D^*$ are strongly correlated. The data are consistent with either small values of the speed parameter σ_D^2 and the threshold D^* or with large values of both parameters.

We can use published information about absolute gene expression levels to refine the likely range of values for these parameters. Promoter and enhancer mutation studies suggest that gene expression levels may be on the order of $10\sigma_m$ to $100\sigma_m$ (Melnikov *et al.* 2012; Patwardhan *et al.* 2012; Metzger *et al.* 2015). The data from Thompson *et al.* (2014), in conjunction with estimates of the distribution of transcript levels in eukaryotic cells (Mortazavi *et al.* 2008; Islam *et al.* 2010; Schwanhäusser *et al.* 2011; Marguerat *et al.* 2012), suggest that a conservative lower limit for D^* is $3\sigma_m$ (see File S3 for details). Letting D^* vary between $3\sigma_m$ and $10^2\sigma_m$, we used the linear regressions shown in Figure 5 to determine a range of plausible values for σ_D^2. We estimate that if only three substitutions of typical size are needed to reduce a paralog's expression to the threshold ($D^* = 3\sigma_m$), then the expected value of σ_D^2 is $5.4 \times 10^{-9}\sigma_m$ per year. If expression is much larger, such that 100 substitutions of typical size are required to reach threshold, then the expected value of σ_D^2 is $1.5 \times 10^{-5}\sigma_m$ per year.

We explored what these results imply about the biological parameters on which the model is based. We began by estimating the strength of dosage-balance selection on the sodium channels. We assumed the range of values for σ_D^2 just described, that μ lies between 10^{-6} and 10^{-4} per allele per generation, that N lies between 10^4 and 10^6, and that there is one generation per year. Equation 4 and these parameter values then imply that the variance of the fitness function ω^2 is between $11\sigma_m^2$ and $4.6 \times 10^6\sigma_m^2$. We can use plausible

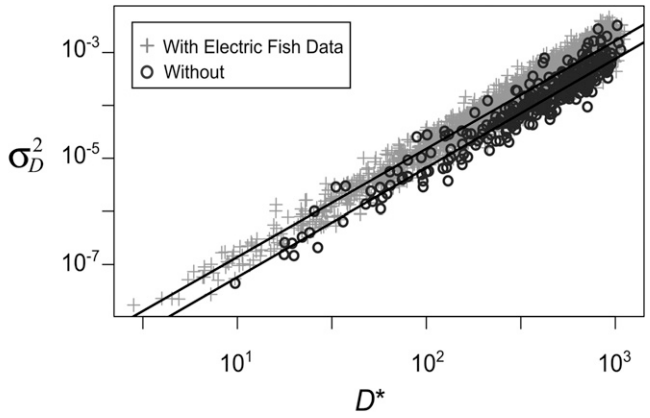

Figure 5 Joint posterior distribution of the diffusion rate parameter σ_D^2 and the expression threshold D^* estimated from sodium channel expression in teleost fish. The joint distributions are from two ABC analyses using the expression data from Thompson *et al.* (2014). In one analysis, the two lineages of electric fish are included, and in the other, they are not. The linear relationship between the parameters from the two analyses is very similar. The regression lines are $\log\sigma_D^2 = 2.04 \log D^* - 20.5$ with the electric fish and $\log\sigma_D^2 = 2.06 \log D^* - 21.3$ without them.

expression levels derived from the studies cited earlier to estimate how efficient dosage-balance selection is at removing expression mutations in terms of transcripts per cell. If the sodium channels are expressed at 50 transcripts per cell and σ_m is 5% of that expression level, for example, then the estimated values of ω^2 imply that mutations that change sodium channel expression by more than 5.3 transcripts per cell are efficiently eliminated by dosage-balance selection.

Next, we asked about the properties of mutations that fix. We simulated the compensatory drift process using the parameter values cited in the preceding paragraph (see File S1 for details). These results show that for small values of D^* ($= 3\sigma_m$) and strong dosage-balance selection ($\omega^2 = 11\sigma_m^2$), 97% of mutations are removed by selection that otherwise would fix. On average, mutations that fix change expression by only $0.02\sigma_m$, and some 9000 substitutions occur before one of the duplicates becomes a pseudogene or neofunctionalizes. For a larger value of D^* ($100\sigma_m$) and very weak selection ($\omega^2 = 4.6 \times 10^6\sigma_m^2$), only 17% of mutations are prevented from fixing by dosage-balance selection. The effect of the average mutation that fixes is $0.7\sigma_m$, and 8000 substitutions occur before the threshold is reached. We emphasize that these estimates are very rough, but they are, to our knowledge, the first for these important evolutionary parameters.

We find that if dosage-balance selection is strong (ω not very much bigger than σ_m), then the parameter estimates for the sodium channels are consistent with the assumptions of one-dimensional diffusion approximation. With weak selection, however, the approximation breaks down. This is so because total expression can deviate substantially from the optimum so that the dynamics are not well approximated by a one-dimensional diffusion. Our model therefore describes the evolutionary dynamics of these sodium channel duplicates if D^* and ω are not very much larger than σ_m but would be more accurately modeled by a two-dimensional diffusion model if they are not. It may be difficult to develop analytic results for this model, but it could be studied numerically.

Stochastic simulations suggest that our results are surprisingly robust to the assumption that no more than one mutation segregates at any given time (*i.e.*, $4N\mu \ll 1$). Simulations of a Wright-Fisher model show that mutations that fix do so largely as a neutral process. The distribution of fitness effects for fixed mutations is shown in File S1. For the parameter values simulated, the mean value of $|Ns|$ is between 0.15 and 0.24, and it is very rare for mutations to fix with $|Ns| > 1$. We ran simulations in which the mutation rate varied over more than four orders of magnitude. When $N\mu = 1$, the most common allele is typically at a frequency of only about 50% (File S2). Nevertheless, the substitution rate is very close to what our model predicts (File S3). This behavior is also consistent with a model in which mutations that segregate at appreciable frequencies are entirely neutral. The results of the simulations begin to significantly depart from the expectations of our model only when $N\mu > 1$. In sum, our analytic results may apply when mutation rates are higher than the approximations assume.

Neofunctionalization and compensatory drift

Because dosage-balance selection can maintain duplicates for long evolutionary periods, it may be more likely that neofunctionalization will occur than it does when dosage balance is weak or absent (Force *et al.* 1999; Papp *et al.* 2003; Aury *et al.* 2006; Hughes *et al.* 2007; Scannell and Wolfe 2008; Thompson *et al.* 2014; Gout and Lynch 2015). To explore this idea further, we extended our model by adding two new kinds of mutations. The first is a loss-of-function mutation that renders one of the duplicates a pseudogene. The probability that it fixes is again given by the fitness function used in the main model. The second kind of mutation neofunctionalizes one of the duplicates. It suffers the same fitness cost as a loss-of-function mutation but also benefits from a 0.1% fitness gain from its new function.

We compared the frequency of neofunctionalization in three simulated populations (File S1) evolving under dosage-balance selection that ranged from strong to very weak: $\omega^2 = 10^2\sigma_m^2$, $10^4\sigma_m^2$, and $10^6\sigma_m^2$. For all three simulations, mutations that alter expression were 10 times more frequent than pseudogenizing mutations, and pseudogenizing mutations were 10^3 times more frequent than neofunctionalizing mutations. The population size was $N = 10^4$, the mutation rate was $\mu = 10^{-5}$ mutations per allele per generation, and the optimal expression was $\theta = 5\sigma_m$.

We found that neofunctionalization is greatly facilitated by dosage-balance selection. Figure 6 shows that when dosage-balance selection is stronger, duplicate genes are preserved for longer, and more mutations occur before a duplicate is lost. In consequence, neofunctionalization happens nearly 10 times more often than when dosage-balance selection is very weak. Neofunctionalization is most likely when expression falls inside a window of values in which the cost of losing

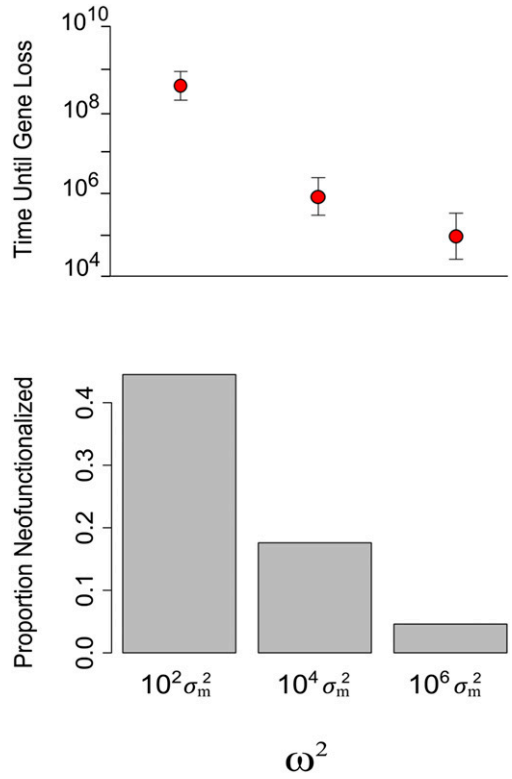

Figure 6 Dosage-balance selection and the probability of neofunctionalization. The top panel shows the number of mutations (a proxy for time) that occur before one of the duplicates neofunctionalizes or pseudogenizes. Dots show the mean, and the whiskers show 1 SD. The bottom panel compares the frequency of neofunctionalization for three strengths of dosage-balance selection, from strong to very weak. Results are based on 10^3 simulations.

the original function is smaller than the benefit of gaining the new function. In this window, a mutation that causes pseudogenization is still too deleterious to fix. Equation 4 shows that stronger dosage-balance selection slows the rate of compensatory drift and thus increases the amount of time the population spends in this evolutionary window. These results suggest that dosage-balance selection greatly diminishes the evolutionary potential of paralogs early after duplication but, after a long period of compensatory drift, greatly facilitates the acquisition of a new adaptive function.

Discussion

We formalized a model of the evolutionary process that we call *compensatory drift*. This model shows how dosage-balance selection on duplicate genes (paralogs) can lead to neofunctionalization some tens to hundreds of millions of years after duplication. Dosage-balance selection constrains the combined expression of both paralogs to an optimum, but not the expression of the individual genes. This allows the relative expression of the paralogs to drift apart by the fixation of mutations with small effects. The speed at which this divergence occurs is determined by the diffusion rate σ_D^2, which, in turn, is a function of several biological parameters. Our results show that stronger dosage-balance selection and larger mutational effects on expression slow divergence because a greater fraction of mutations is strongly deleterious and so has virtually no chance of fixation. Larger populations also decrease divergence because they enhance the efficiency of selection and so eliminate a larger fraction of mutations.

Simulations of compensatory drift reveal that dosage-balance selection can improve the odds that neofunctionalization occurs rather than pseudogenization. If a novel function yields a slight advantage while having a large tradeoff with the ancestral function, dosage-balance selection can still improve the chances of neofunctionalization, but only after a long period of compensatory drift. As expression of one paralog declines, the strength of selection to maintain its original function diminishes. It reaches a level at which mutations that pseudogenize the gene are still strongly deleterious, but mutations that neofunctionalize are beneficial. Our results show that the probability of neofunctionalization is increased when the added expression of duplicates is high, dosage-balance constraints are strong, and population sizes are large.

We fit the model to data on sodium channel duplicates in teleost fish. We estimate that the diffusion rate σ_D^2 lies between $5.4 \times 10^{-9}\sigma_m^2$ and $1.5 \times 10^{-5}\sigma_m^2$ per year, where σ_m^2 is the variance of mutation effect sizes. The square root of σ_D^2 is roughly equal to the amount of divergence that accumulates in a lineage per year. This implies that duplicates diverge between $7 \times 10^{-5}\overline{\delta}$ and $4 \times 10^{-3}\overline{\delta}$ per year, where $\overline{\delta}$ is the average effect that a mutation has on the amount of gene product produced by a duplicate. About 8000–9000 substitutions occur before the threshold is reached. This number seems large, but it is not inconceivable. Summing up all the genetic elements that can affect expression (*e.g.*, promoters, enhancers, microRNAs, post-translational regulators, etc.), there are many mutational targets for expression changes. Indeed, high rates of enhancer gain and loss (enhancer turnover) have been seen in several taxa (Schmidt *et al.* 2010; Domene *et al.* 2013; Paris *et al.* 2013; Arnold *et al.* 2014). Dosage-balanced duplicates may undergo more rapid enhancer turnover than singleton genes because compensation is possible at two different loci. A last consideration is that the time span involved is long, on the order of 10^8 generations. In any event, our inferences about numbers of substitutions are very imprecise, and the actual number may be much smaller. In the future, we expect that larger data sets of comparative paralog expression will emerge and will allow greater precision in parameter estimates using methods of analysis such as ABC.

This work builds on earlier hypotheses about the evolution of dosage-sensitive duplicates. Aury *et al.* (2006) proposed that expression of duplicates evolves by compensatory changes, which can greatly delay the pseudogenization or neofunctionalization of one of the pair. Later work suggested that this process leads to a "random walk" along a line of equal combined expression, a process that could explain comparative gene expression patterns observed in disparate lineages of organisms (Thompson *et al.* 2014; Gout and Lynch

2015; Lan and Pritchard 2015). Other researchers suggested that gene loss in a duplicated network would cause imbalances and thus put positive selective pressure for loss of other duplicates in the same network, leading to concerted duplicate inactivation (Papp *et al.* 2003; Hughes *et al.* 2007; Konrad *et al.* 2011). Under compensatory drift, the eventual loss of a duplicate may not have much impact on other genes in its network because its paralog will already be producing (almost) all the gene product needed.

Several lines of evidence are consistent with dosage-balance selection after WGD. In contrast to classical models in which redundant duplicates evolve neutrally (Ohno 1970; Walsh 1995; Force *et al.* 1999; Lynch and Conery 2000), dosage-balance selection will cause both genes to be essential immediately after duplication. WGD does not disrupt dosage balance, and therefore, many preserved duplicates originating in a WGD may evolve under dosage-balance selection. *Paramecium tetraurelia* has undergone three WGDs in its evolutionary history. In a large proportion of the duplicates from the most recent WGD, both members of the pair are evolving under strong purifying selection, and this proportion declines over time (Aury *et al.* 2006). This pattern indicates that many genes are dosage sensitive and evolve under dosage-balance selection but that eventually selection to conserve function is lost for one of the duplicates. Other examples come from vertebrates. Some 100 million years after a WGD in the ancestor of salmonid fish, about half the duplicates are retained, and one-quarter of those are still similar in expression and sequence (Berthelot *et al.* 2014). In a WGD that happened in the ancestor of teleost fish about 300 million years ago, many duplicate pairs persisted for over 200 million years before a member of the pair was lost (Blomme *et al.* 2006; Brunet *et al.* 2006; Sato *et al.* 2009). Delayed loss of duplicates long after a WGD is also seen in *Paramecium* species (McGrath *et al.* 2014b). Together these patterns indicate that many duplicates after WGDs are dosage sensitive and evolve in two phases: an initial prolonged phase where both duplicates evolve under selection that conserves function and a later phase in which a duplicate is lost. This later phase could be due to a paralog drifting to low expression and may be the stage at which a redundant gene is most likely to evolve a new function.

Additional predictions flow from the compensatory drift model. Duplicate pairs should persist longer if their total expression is high because more mutations must fix to reach the expression threshold p^* (*i.e.*, D^* is larger). (Figure 4 shows the impact of increasing D^* on the time until duplicate loss.) Both yeast and paramecia show just this pattern: there is a positive correlation between expression levels and the longevity of duplicated genes following WGD (Seoighe and Wolfe 1999; Aury *et al.* 2006; Gout *et al.* 2010; McGrath *et al.* 2014b). To explain this pattern, Gout *et al.* (2010) argued that stabilizing selection on total expression is stronger on dosage-sensitive duplicates that have high levels of expression. This idea is consistent with our model: the speed at which expression of paralogs diverges becomes slower as the strength of selection increases. The model also makes predictions about patterns of subfunctionalization of dosage-balanced duplicates. When duplicates are expressed in different cell types under different regulation, compensatory drift can occur in parallel in the two cell types, occasionally leading to subfunctionalized expression. Finally, our model makes predictions about phylogenetic patterns. We expect the member of a duplicate pair that has neofunctionalized in a lineage to have lower expression than its paralog in closely related lineages where neofunctionalization has not occurred (Anderson and Evans 2009; Thompson *et al.* 2014). Recent data support this prediction (Gout and Lynch 2015).

Compensatory drift may play an important role in two other evolutionary contexts. Dosage-balance selection can act on gene duplicates that do not arise by WGD. Selection for increased expression can fix a duplicated gene in a population (Kondrashov 2012). Subsequently, there is stabilizing selection favoring the new, higher-expression optimum. Once this level is reached, the expression can diverge by compensatory drift, as described by our model. Second, compensatory drift can act on the transcription and translation rates for a gene evolving under stabilizing selection for expression. An important difference with duplicate genes is that transcription and translation rates cannot completely compensate for each other. Qualitatively, however, we expect to see similar evolutionary dynamics.

In our model, neofunctionalization happens after a long period of compensatory drift. Alternatively, a novel gene function could predate the duplication event as a minor pleiotropic effect that is not optimized because of tradeoffs. Under the escape-from-adaptive-conflict model, duplicates are freed from these tradeoffs, allowing one of them to become rapidly optimized for the alternative function (Conant and Wolfe 2008; Des Marais and Rausher 2008). However, if one of the gene's functions requires both duplicates to contribute expression, then compensatory drift would have to occur before one duplicate can escape from the adaptive conflict.

Compensatory drift is related to but distinct from quantitative subfunctionalization (QS). This process describes how, following duplication, degenerative mutations accumulate by drift in each paralog until their total expression declines to a minimum total level necessary for viability (Force *et al.* 1999, Stoltzfus 1999, Lynch and Force 2000, Hahn 2009; Qian *et al.* 2010). Compensatory drift, in contrast, is the divergence of expression in paralogs that have already reached optimal expression under dosage-balance selection. A second difference between the processes is that under compensatory drift, half the mutations that fix increase expression, while under QS, none of them do. Despite these differences, there are also important similarities. Both processes can dramatically increase the probability that a gene neofunctionalizes. The two processes could operate in succession. Following the tandem duplication of a gene, expression of each duplicate can decline until both paralogs are necessary to produce the minimal expression needed. The duplicates then can diverge through compensatory drift.

Dosage-balance selection may provide opportunities for adaptation long after WGD occurs. When one of a duplicate pair of genes drifts to a low level of expression, a period of incubation occurs during which it can evolve a new function. As illustrated by duplicates of sodium channel genes in teleost fish, downregulation of dosage-sensitive duplicates may be a common preadaptation in many diversifying gene families. Compensatory drift thus still may be facilitating adaptation very long after the two WGDs that occurred near the root of the vertebrate tree.

Acknowledgments

We thank Laura Crothers for comments on the manuscript. We also acknowledge the Texas Advanced Computing Center (TACC) at the University of Texas at Austin for providing HPC resources that have contributed to the research results reported in this paper. This research was funded by National Science Foundation grants DEB-1311521 to A.T. and DEB-0819901 to M.K.

Literature Cited

Arnold, C. D., D. Gerlach, D. Spies, J. A. Matts, Y. A. Sytnikova *et al.*, 2014 Quantitative genome-wide enhancer activity maps for five Drosophila species show functional enhancer conservation and turnover during cis-regulatory evolution. Nat. Genet. 46: 685–692.

Anderson, D. W., and B. J. Evans, 2009 Regulatory evolution of a duplicated heterodimer across species and tissues of allopolyploid clawed frogs (Xenopus). J. Mol. Evol. 68: 236–247.

Arnegard, M. E., D. J. Zwickl, Y. Lu, and H. H. Zakon, 2010 Old gene duplication facilitates origin and diversification of an innovative communication system—twice. Proc. Natl. Acad. Sci. USA 107: 22172–22177.

Aury, J., O. Jaillon, L. Duret, B. Noel, C. Jubin *et al.*, 2006 Global trends of whole-genome duplications revealed by the ciliate *Paramecium tetraurelia*. Nature 444: 171–178.

Beaumont, M. A., 2010 Approximate Bayesian computation in evolution and ecology. Annu. Rev. Ecol. Evol. Syst. 41: 379–406.

Beaumont, M. A., W. Zhang, and D. J. Balding, 2002 Approximate Bayesian computation in population genetics. Genetics 162: 2025–2035.

Berthelot, C., F. Brunet, D. Chalopin, A. Juanchich, M. Bernard *et al.*, 2014 The rainbow trout genome provides novel insights into evolution after whole-genome duplication in vertebrates. Nat. Commun. 5: 1–10.

Betancur-R, R., R. E. Broughton, E. O. Wiley, K. Carpenter, J. A. López *et al.*, 2013 The tree of life and a new classification of bony fishes. PLoS Curr. 5: pii: ecurrents.tol.53ba26640df0ccaee75bb165c8c26288.

Birchler, J. A., and R. A. Veitia, 2012 Gene balance hypothesis: connecting issues of dosage sensitivity across biological disciplines. Proc. Natl. Acad. Sci. USA 109: 14746–14753.

Birchler, J. A., U. Bhadra, M. P. Bhadra, and D. L. Auger, 2001 Dosage-dependent gene regulation in multicellular eukaryotes: implications for dosage compensation, aneuploidy syndromes and quantitative traits. Dev. Biol. 234: 275–288.

Birchler, J. A., N. C. Riddle, D. L. Auger, and R. A. Veitia, 2005 Dosage balance in gene regulation: biological implications. Trends Genet. 21: 219–226.

Blomme, T., K. Vandepoele, S. De Bodt, C. Simillion, S. Maere *et al.*, 2006 The gain and loss of genes during 600 million years of vertebrate evolution. Genome Biol. 7: R43.

Brunet, F. G., H. R. Crollius, M. Paris, J. Aury, P. Gilbert *et al.*, 2006 Gene loss and evolutionary rates following whole-genome duplication in teleost fishes. Mol. Biol. Evol. 23: 1808–1816.

Conant, G. C., and K. H. Wolfe, 2008 Turning a hobby into a job: how duplicated genes find new functions. Nat. Rev. Genet. 9: 938–950.

Cox, D. R., and H. D. Miller, 1965 Markov processes in continuous time with continuous state space, pp. 203–251 in *The Theory* of *Stochastic Processes*. Wiley, New York.

Des Marais, D. L., and M. D. Rausher, 2008 Escape from adaptive conflict after duplication in an anthocyanin pathway gene. Nature 454: 762–765.

Domene, S., V. F. Bumaschy, F. S. J. de Souza, L. F. Franchini, S. Nasif *et al.*, 2013 Enhancer turnover and conserved regulatory function in vertebrate evolution. Phil. Trans. R. Soc. Lond. B Biol. Sci. 368: 20130027.

Edger, P. P., and J. C. Pires, 2009 Gene and genome duplications: the impact of dosage-sensitivity on the fate of nuclear genes. Chromosome Res. 17: 699–717.

Felsenstein, J., 1985 Phylogenies and the comparative method. Am. Nat. 125: 1–15.

Force, A., M. Lynch, F. B. Pickett, A. Amores, Y. Yan *et al.*, 1999 Preservation of duplicate genes by complementary, degenerative mutations. Genetics 151: 1531–1545.

Freeling, M., and B. C. Thomas, 2006 Gene-balanced duplications, like tetraploidy, provide predictable drive to increase morphological complexity. Genome Res. 16: 805–814.

Gout, J.-F., and M. Lynch, 2015 Maintenance and loss of duplicated genes by dosage subfunctionalization. Mol. Biol. Evol. 32: 2141–2148.

Gout, J., D. Kahn, and L. Duret Paramecium Post-Genomics Consortium, 2010 The relationship among gene expression, the evolution of gene dosage, and the rate of protein evolution. PLoS Genet. 6: e1000944.

Hahn, M. W., 2009 Distinguishing among evolutionary models for the maintenance of gene duplicates. J. Hered. 100: 605–617.

Haldane, J. B. S., 1933 The part played by recurrent mutation in evolution. Am. Nat. 67: 5–19.

He, X., and J. Zhang, 2005 Rapid subfunctionalization accompanied by prolonged and substantial neofunctionalization in duplicate gene evolution. Genetics 169: 1157–1164.

Hughes, T., D. Ekman, H. Ardawatia, A. Elofsson, and D. A. Liberles, 2007 Evaluating dosage compensation as a cause of duplicate gene retention in Paramecium tetraurelia. Genome Biol. 8: 213.

Islam, S., U. Kjällquist, A. Moliner, P. Zajac, J.-B. Fan *et al.*, 2011 Characterization of the single-cell transcriptional landscape by highly multiplex RNA-seq. Genome Res. 21: 1160–1167.

Kimura, M., 1962 On the probability of fixation of mutant genes in a population. Genetics 47: 713–719.

Kondrashov, F. A., 2012 Gene duplication as a mechanism of genomic adaptation to a changing environment. Proc. Biol. Sci. 279: 5048–5057.

Konrad, A., A. I. Teufel, J. A. Grahnen, and D. A. Liberles, 2011 Toward a general model for the evolutionary dynamics of duplicate genes. Genome Biol. Evol. 3: 1197–1209.

Lan, X., and J. K. Pritchard, 2015 Long-term survival of duplicate genes despite absence of subfunctionalized expression. bioRxiv DOI: 10.1101/019166

Lavoué, S., M. Miya, M. E. Arnegard, J. P. Sullivan, C. D. Hopkins *et al.*, 2012 Comparable ages for the independent origins of electrogenesis in African and South American weakly electric fishes. PLoS One 7: e36287.

Lynch, M., and J. S. Conery, 2000 The evolutionary fate and consequences of duplicate genes. Science 290: 1151–1155.
Lynch, M., and A. Force, 2000 The probability of duplicate gene preservation by subfunctionalization. Genetics 154: 459–473.
Makino, T., and A. McLysaght, 2010 Ohnologs in the human genome are dosage balanced and frequently associated with disease. Proc. Natl. Acad. Sci. USA 107: 9270–9274.
Marguerat, S., A. Schmidt, S. Codlin, W. Chen, R. Aebersold *et al.*, 2012 Quantitative Analysis of Fission Yeast Transcriptomes and Proteomes in Proliferating and Quiescent Cells. Cell 151: 671–683.
McGrath, C. L., J. F. Gout, T. G. Doak, A. Yanagi, and M. Lynch, 2014a Insights into three whole-genome duplications gleaned from the Paramecium caudatum genome sequence. Genetics 197: 1417–1428.
McGrath, C. L., J.-F. Gout, P. Johri, T. G. Doak, and M. Lynch, 2014b Differential retention and divergent resolution of duplicate genes following whole-genome duplication. Genome Res. 24: 1665–1675.
Melnikov, A., A. Murugan, X. Zhang, T. Tesileanu, L. Wang *et al.*, 2012 Systematic dissection and optimization of inducible enhancers in human cells using a massively parallel reporter assay. Nat. Biotechnol. 30: 271–277.
Metzger, B. P. H., D. C. Yuan, J. D. Gruber, F. Duveau, and P. J. Wittkopp, 2015 Selection on noise constrains variation in a eukaryotic promoter. Nature 521: 344–347.
Mortazavi, A., B. A. Williams, K. McCue, L. Schaeffer, and B. Wold, 2008 Mapping and quantifying mammalian transcriptomes by RNA-seq. Nat. Methods 5: 621–628.
Muller, H. J., 1936 Bar duplication. Science 83: 528–530.
Novak, A., M. Jost, Y. Lu, A. Taylor, H. H. Zakon *et al.*, 2006 Gene duplications and evolution of vertebrate voltage-gated sodium channels. J. Mol. Evol. 63: 208–221.
Ohno, S., 1970 *Evolution by Gene Duplication*. Springer-Verlag, New York.
Ohta, T., 1987 Simulating evolution by gene duplication. Genetics 115: 207–213.
Papp, B., C. Pal, and L. D. Hurst, 2003 Dosage sensitivity and the evolution of gene families in yeast. Nature 424: 194–197.
Paris, M., T. Kaplan, X. Y. Li, J. E. Villalta, S. E. Lott *et al.*, 2013 Extensive divergence of transcription factor binding in Drosophila embryos with highly conserved gene expression. PLoS Genet. 9: e1003748.
Patwardhan, R. P., J. B. Hiatt, D. M. Witten, M. J. Kim, R. P. Smith *et al.*, 2012 Massively parallel functional dissection of mammalian enhancers in vivo. Nat. Biotechnol. 30: 265–270.
Qian, W., and J. Zhang, 2008 Gene dosage and gene duplicability. Genetics 179: 2319–2324.
Qian, W., B. Liao, A. Y. Chang, and J. Zhang, 2010 Maintenance of duplicate genes and their functional redundancy by reduced expression. Cell 26: 425–430.
Rastogi, S., and D. A. Liberles, 2005 Subfunctionalization of duplicated genes as a transition state to neofunctionalization. BMC Evol. Biol. 5: 28.
Sato, Y., Y. Hashiguchi, and M. Nishida, 2009 Temporal pattern of loss/persistence of duplicate genes involved in signal transduction and metabolic pathways after teleost-specific genome duplication. BMC Evol. Biol. 9: 127.
Scannell, D. R., and K. H. Wolfe, 2008 A burst of protein sequence evolution and a prolonged period of asymmetric evolution follow gene duplication in yeast. Genome Res. 18: 137–147.
Schmidt, D., M. D. Wilson, B. Ballester, P. C. Schwalie, G. D. Brown *et al.*, 2010 Five-vertebrate ChIP-seq reveals the evolutionary dynamics of transcription factor binding. Science 328: 1036–1040.
Schwanhäusser, B., D. Busse, N. Li, G. Dittmar, J. Schuchhardt *et al.*, 2011 Global quantification of mammalian gene expression control. Nature 473: 337–342.
Seoighe, C., and K. H. Wolfe, 1999 Yeast genome evolution in the post-genome era. Curr. Opin. Microbiol. 2: 548–554.
Stoltzfus, A., 1999 On the possibility of constructive neutral evolution. J. Mol. Evol. 49: 169–181.
Stranger, B. E., M. S. Forrest, M. Dunning, C. E. Ingle, C. Beazley *et al.*, 2007 Relative impact of nucleotide and copy number variation on gene expression phenotypes. Science 315: 848–853.
Tavare, S., D. J. Balding, R. C. Griffiths, and P. Donnelly, 1997 Inferring coalescence times from DNA sequence data. Genetics 145: 505–518.
Thompson, A., D. Vo, C. Comfort, and H. H. Zakon, 2014 Expression evolution facilitated the convergent neofunctionalization of a sodium channel gene. Mol. Biol. Evol. 31: 1941–1955.
Veitia, R. A., 2002 Exploring the etiology of haploinsufficiency. BioEssays 24: 175–184.
Walsh, B., 2003 Population-genetic models of the fates of duplicate genes. Genetica 118: 279–294.
Walsh, J. B., 1995 How often do duplicated genes evolve new functions? Genetics 139: 421–428.
Zakon, H. H., Y. Lu, D. J. Zwickl, and D. M. Hillis, 2006 Sodium channel genes and the evolution of diversity in communication signals of electric fishes: convergent molecular evolution. Proc. Natl. Acad. Sci. USA 103: 3675–3680.

Communicating editor: J. Wakeley

GENETICS

Supporting Information
www.genetics.org/lookup/suppl/doi:10.1534/genetics.115.178137/-/DC1

Compensatory Drift and the Evolutionary Dynamics of Dosage-Sensitive Duplicate Genes

Ammon Thompson, Harold H. Zakon, and Mark Kirkpatrick

DOI: 10.1534/genetics.115.178137

File S1

Stochastic Simulation of Compensatory Drift

Stochastic simulations for the evolution of p_1 and p_2

We used explicit stochastic simulations of compensatory drift to check the diffusion approximation and gain additional insight about the evolutionary process. In our simulations, expression-altering mutations appeared in diploid individuals in a population of size N at a mutation rate μ per allele per generation. The initial conditions were $p_1 = p_2$ and $p_1 + p_2 = \theta$, where θ is the optimal expression level. Expression evolved according to a Poisson process. The number of generations until the next mutation appeared in an individual in the population was drawn from an exponential distribution with rate parameter $\lambda = 4N\mu$. Mutations occurred in either duplicate with equal probability and changed expression of that duplicate by a random amount, δ, drawn from a standard normal distribution. The selection coefficient for a mutation that changes p_2 to $p_2 + \delta$ was calculated as $s = \frac{W(p_1,p_2+\delta)}{W(p_1,p_2)} - 1$, where $W()$ is the fitness function given by equation 1 in File S2. The probability that the mutation fixed was calculated with Equation 1 from the main text. If the mutation fixed, then expression in the population for that duplicate was updated and the process began again. Absorption occurred when the expression of one of the duplicates fell below the threshold at p^* or rose above the threshold at $\theta - p^*$. Mutation effect size is independent of distance from the threshold. The amount of the mutation density that extends beyond the threshold is the probability of a mutation that guarantees a neofunctionalizing or pseudogenizing event. This also means that the total density that extends into negative expression is treated as the probability of a mutation that completely turns off expression. In the event the threshold is reached, regardless of which duplicate crossed a threshold, the duplicate with lower expression neofunctionalized or pseudogenized.

To check the diffusion approximation, we simulated compensatory drift within a single lineage for different numbers of generations and different values of the parameters (μ, N, ω^2). We generated empirical distributions for the difference in expression, $D = p_1 - p_2$, and compared them to the diffusion approximations given by Equations 5 and 6 in the main text. Results showed that the simulations and diffusion approximation agreed closely.

We also used the simulations to confirm the assumption made by the diffusion approximation that the sum of expression, $A = p_1 + p_2$, tends to stay close to the optimum value, θ. We used the range of parameter values estimated from our ABC analysis to simulate expression evolution under the model and measure the standard deviation of *A*, which we denote as σ_A. We found that σ_A is small compared to σ_m and θ when selection is at least strong enough to remove approximately half of expression altering mutations.

To gain additional insight about compensatory drift, we used the simulations to find the number of mutations, number of mutations that fix, and the sizes of mutations that fix. The results are reported in the main text. We measured the proportion of all mutations that fix under these parameter values, which we call α, and used this value to measure the proportion of mutations that were prevented from fixing by dosage-balance selection. We calculated that proportion as $1 - 2N\alpha$.

Dosage balance selection and the probability of neofunctionalization

To study the frequency of neofunctionalization under compensatory drift, we simulated the dynamics as above. These simulations included two more types of mutations, pseudogenizing and neofunctionalizing. We set the pseudogenization mutation rate to be 10^3 times higher than the neofunctionalization rate. Ten percent of mutations were pseudogenizing, and 0.01% of mutations caused neofunctionalization. Neofunctionalization increased fitness by 0.1% but also caused a loss of fitness since expression no longer contributed to the ancestral function. The fitness of a pseudogenizing mutation, for example if p_1 became a pseudogene leaving p_2 alone to contribute expression, was calculated as $W = \exp\left[\frac{-(p_2-\theta)^2}{2\omega^2}\right]$ and if p_1 had neofunctionalized then $W = 1.001 \times \exp\left[\frac{-(p_2-\theta)^2}{2\omega^2}\right]$. The only parameter that was varied in the simulations was the selection strength ω^2, which took the values of $10^2\,\sigma_m^2$, $10^4\,\sigma_m^2$, and $10^6\,\sigma_m^2$. One thousand simulations were run for each condition. Simulations ended when either pseudogenization or neofunctionalization of one of the duplicates had occurred.

Substitution in populations with high $N\mu$

If the mutation rate is high and/or the population size is large, the population is likely to be polymorphic when a mutation appears in that population, which violates the assumption of our

analytic model. If most mutations that reach an appreciable frequency in the population are effectively neutral, then we expect this fact to have a negligible impact on the rate of substitutions. To assess this issue we performed stochastic simulations as described above and recorded the values of *Ns* for mutations that fix. We simulated populations with three strengths of selection, corresponding to situations in which 99%, 90%, or 50% of mutations have $|Ns| > 1$. Figure S1 shows the distribution of *Ns* of mutations that fixed. The mean $|Ns|$ of mutations that fix was 0.24 (median = 0.15) for all three cases. Less than 1.3% of substitutions had $|Ns| > 1$. In summary, simulations show that more than 98% of mutations that fix are nearly neutral even when 99% of random mutations have a large impact on fitness ($|Ns| > 1$).

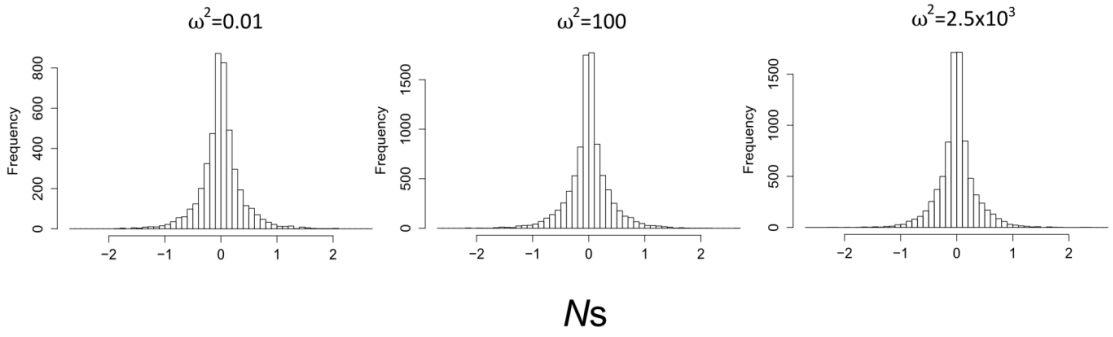

Figure S1. Distribution of *Ns* for fixed mutations. Stochastic simulations of a population of size $N = 10^4$, mutation rate $\mu = 10^{-4}$, and $\theta = 100$. Three different strengths of dosage balance selection were simulated. The selection parameter (ω^2) value used for each simulation is indicated above each distribution.

These results indicate that the vast majority of mutations that fix are nearly neutral, suggesting that the model may provide a good approximation even when population size and/or mutation are large.

To investigate this issue further, we performed individual-based simulations. If substitution is a Poisson process, then the mean number of substitutions will have a linear relationship with the mutation rate. If high mutation rates impact the dynamics of substitution, then the mean number of substitution should depart from that linear relationship as $N\mu$ becomes high relative to the time it takes for a mutation to fix.

We simulated populations of $N = 100$ asexual haploid individuals evolving by non-overlapping generations for 10^6 generations. Each individual had a probability μ of mutating. If mutation happened in an individual then a random variate δ was drawn from a standard Normal distribution and was added to the expression level of the individual. Zygotes were created for generation $t + 1$ by sampling individuals in generation t with probabilities proportional to their fitnesses. Selection strength was such that 62% of mutations had $|Ns| > 1$. The starting condition was all individuals in the population had optimal expression.

Simulations were run for values of $N\mu$ over the range $[10^{-4}, 10]$. We determined the allele frequency spectra by sampling the simulations every 10^3 generations, and calculated the substitution rates. The results for the allele frequency spectra are shown in Figure S2. With $N\mu = 0.1$, the most common allele was typically at a frequency around 85%, and no more than four alleles segregated. With $N\mu = 1$, the major allele frequency is typically 50%, and up to 12 alleles segregate.

The relationship between $N\mu$ and the substitution rate is shown in Figure S3. The relation at higher mutation rates is very close to what is expected from extrapolating from the lowest mutation rates (the regime where our Poisson process approximation holds). At the very highest mutation rates ($N\mu > 1$), we begin to see departures from linearity, but the departures are still not large even with $N\mu = 10$. We conclude that our model provides good approximations for mutation rates that are somewhat higher than are justified by our assumption that only one mutation segregates at a time.

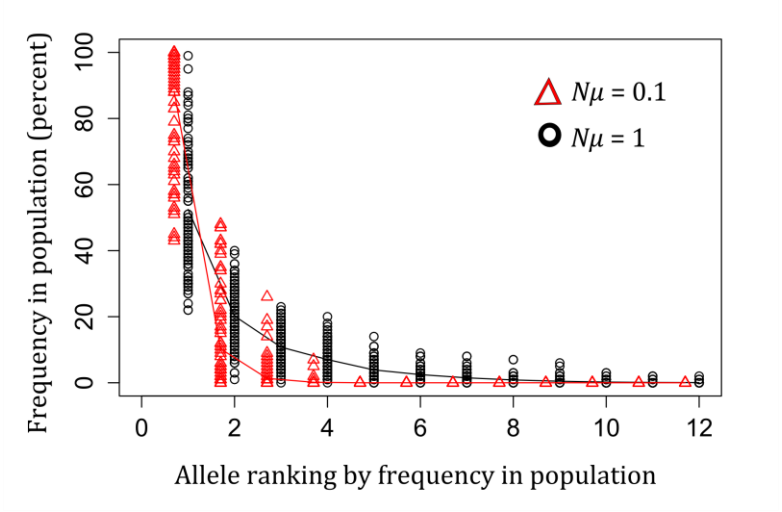

Figure S2. Frequency spectrum of segregating alleles. The results of two simulations with $N\mu$ = 0.1 (red triangles) and 1 (black circles). The population was sampled every 10^3 generations over the course of 10^5 generations. Each point is the frequency of an allele in the population with a particular frequency ranking. The most common allele is ranked 1, the second most common ranked 2, etc. The lines indicate the mean allele frequency of a given ranking for the whole simulation.

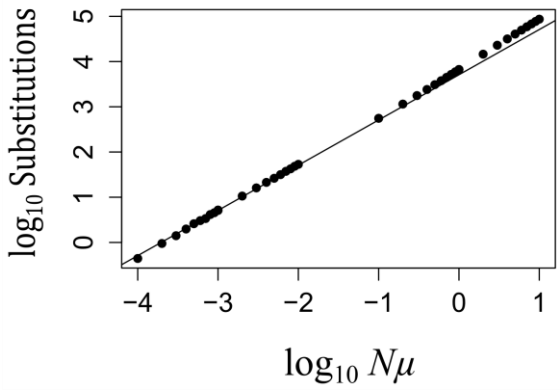

Figure S3. Substitution rate and mutation rate. Each point shows the mean number of substations in 10^3 replicate simulations for 40 different values of $N\mu$. A line of slope 1 was fit to the results of simulations with the lowest $N\mu$ between 10^{-4} and 10^{-2} where independent mutations largely do not co-segregate in the population. Departure from this line at higher $N\mu$ indicates that interference between mutations co-segregating in the population is impacting the substitution rate. The deviation is, however, not large over this range of parameters.

File S2

Compensatory drift and the evolutionary dynamics of dosage-sensitive duplicate genes

The model

Stabilizing selection acts on the total expression of two paralogous genes. The expression levels of the genes are denoted p_1 and p_2. The fitness function is:

$$W = \exp\left[\frac{-(p_1+p_2-\theta)^2}{2\omega^2}\right] \quad (1)$$

where θ is the optimum for the sum $p_1 + p_2$, and ω^2 is the width (variance) of the fitness function, and so larger values imply weaker selection. (Equation (1) can be viewed as an approximation for a wide range of stabilizing fitness functions, including asymmetric ones, if ω^2 is chosen to produce the same curvature along the diagonal. The approximation will be best when parameters are such that total gene expression stays near the optimum: $p_1 + p_2 \approx \theta$). In graphical form the fitness function looks like this:

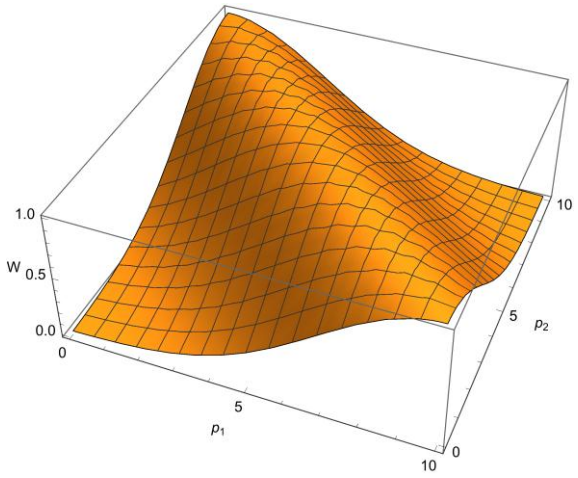

We assume that there is a threshold of expression. Above this threshold, a paralog cannot become a pseudogene or neofunctionalize because the fitness cost to its original function would be too great. Below the threshold, however, neofunctionalization or pseudogenization is guaranteed to happen, and it happens on a fast timescale relative to the speed at which the *p*s change. We denote the threshold as *p**.

When a mutation that changes expression occurs, one of the two loci is chosen at random to mutate. We assume that the distribution of mutational effects on expression, denoted $f_\mu()$, is

normal with mean 0 and variance σ_m^2. The probability that a mutation with an effect δ on either p_1 or p_2 fixes is denoted $P_{fix}(\delta)$. There is a probability μ per generation that a mutation affecting expression will occur at each of the two gene copies at each of the two paralogs. The waiting time until the next mutation appears in the population is exponentially-distributed with mean $1/(4N\mu)$. The evolutionary dynamics therefore proceed as a random walk in p_1 and p_2.

A diffusion approximation

It is useful to work in terms of the sum *A* and the difference *D* in expression at the two loci:

$$\begin{aligned} A &= p_1 + p_2 \\ D &= p_1 - p_2 \end{aligned} \qquad (2)$$

There are two reasons for this change of variables. Stabilizing selection acts on *A* but is indifferent to *D*, and that fact simplifies the derivation below. Second, our data are on *D* (see File S3), and so this parameterization focuses our attention in the model on the quantity of empirical interest.

In the absence of boundary conditions (that is, with no neofunctionalization), the density function for *A* and *D* can be written as the product of independent density functions:

$$f_{A,D} = f_A(A) f_D(D) \qquad (3)$$

That relation also holds approximately when neofunctionalization does happen if stabilizing selection is strong relative to drift. Then the value of *A* will stay very close to its optimal value. The evolutionary dynamics then lie (almost) along a single dimension in which $A = \theta$ and the difference in expression, *D* diverges with time. This is the key approximation to what follows. We will therefore assume this situation holds, and proceed to develop a partial differential equation (PDE) for the density function $f_D()$. Simulations described in File S1 validate the accuracy of this approximation over the parameter values of biological interest to us. The PDE for *D* follows that of simple Brownian motion:

$$\partial_t f_D = \frac{1}{2}\sigma_D^2 \partial_{D,D} f_D \qquad (4)$$

The diffusion coefficient σ_D^2 determines the evolutionary rate at which *D* will diverge in the paralogs.

Calculating the diffusion coefficient

The diffusion coefficient is defined as the instantaneous rate of increase in the variance of *D*, the difference of expression in the paralogs. We calculate that rate as

$$\sigma_D^2 = \int \left(\delta - \bar{\delta}\right)^2 [4N\mu f_\mu(\delta)] P_{fix}(\delta) d\delta \quad (5)$$

where $\bar{\delta}$ is the mean effect of mutations that fix, which is approximately 0. The term in square brackets represents the number of new mutations with effect δ entering the population each generation. $P_{fix}(\delta)$ is the probability that a mutation with effect δ fixes, for which we use Kimura's (1964) approximation:

$$P_{\text{fix}}(\delta) = \frac{1-\exp[-2s(\delta)]}{1-\exp[-4Ns(\delta)]} \quad (6)$$

Here $s(\delta)$ is the relative fitness of a mutation with an effect δ on expression:

$$s(\delta) \approx \frac{W(\delta)}{W(0)} - 1 \quad (7)$$

$$\approx \exp\left[\frac{-\delta^2}{2\omega^2}\right] - 1 \approx \frac{-\delta^2}{2\omega^2} \quad (8)$$

Equation (7) makes use of the earlier assumption that selection is sufficiently strong relative to drift that *A* is typically very close to θ.

Combining these expressions gives us

$$\sigma_D^2 = \frac{4N\mu}{\sqrt{2\pi}\sigma_m} \int \delta^2 \exp\left[\frac{-\delta^2}{2\sigma_m^2}\right] \left(\frac{\exp\left[\frac{\delta^2}{\omega^2}\right]-1}{\exp\left[\frac{2\delta^2 N}{\omega^2}\right]-1} \right) d\delta \quad (9)$$

That integral cannot be solved analytically. We can, however, determine its value using the following combination of analytic and numerical arguments. The probability that a mutation fixes is close to that for a neutral mutation (= 1/2*N*) if the magnitude of its selection coefficient is sufficiently small, while the probability becomes negligible if the selection coefficient is larger than that. From basic population genetics, we know that this critical value for the selection coefficient is *c*/2*N*, where *c* is an unknown constant that is approximately equal to 1 (Crow and Kimura, 1970). Using δ^* to denote the mutational effect corresponding to that selection coefficient, we find from Equation (8) that

$$\delta^* = \sqrt{\frac{c\omega^2}{N}}. \tag{10}$$

Now assume that the average size of mutational effects is much greater than δ^*, in which case $f_\mu(\delta) \approx f_\mu(0)$ for $-\delta^* < \delta < \delta^*$. Equation (9) for the diffusion coefficient is now

$$\sigma_D^2 \approx 4N\mu \int_{-\delta^*}^{\delta^*} \delta^2 f_\mu(\delta) \left(\frac{1}{2N}\right) d\delta \tag{11}$$

$$\approx k \frac{\mu\omega^3}{\sigma_m N^{3/2}} \ , \tag{12}$$

where *k* is a numerical constant that is independent of all of the model's parameters.

The last element needed is the value of *k*. While we could resort to further analytic approximations, we chose to determine the value for *k* using stochastic simulations. We simulated a random walk in p_1 and p_2 (or equivalently, in *A* and *D*) in the absence of absorbing boundaries at $p = p^*$ and $\theta - p^*$. We calculated the variance among replicate simulations at time *t* and fit *k* using the fact that under Equation (4) we expect

$$Var[D] = \sigma_D^2 t. \tag{13}$$

We find that $k \approx 1.543$. We verified that consistent results are obtained from simulations using different values for $\mu, \omega^2, \sigma_m^2$, and *N* so long as the resulting value for σ_D^2 as given by Equation (12) is unaltered.

References

Crow, J. F. and M. Kimura, 1970 An Introduction to Population Genetics. New York: Harper & Row.

File S3

ABC analysis of the sodium channel expression data

We estimated the posterior distributions of the two model parameters, σ_D^2 and D^* from the comparative expression data in Thompson *et al.* (2014) using Approximate Bayesian Computation, or ABC. The approach follows three steps. First, model parameters (e.g. σ_D^2 and D^*) are drawn from prior distributions. Second, data is simulated using the model and selected parameter values. Third, results from the simulation are compared to the real dataset using summary statistics; parameters that yield results sufficiently similar to the real data are retained, while the others are rejected from the posterior distribution.

We implemented ABC by simulating the diffusion approximation described in the text. We first selected uninformative prior distributions for the two model parameters. For σ_D^2 the prior distribution was $f(\sigma_D^2) = 1/(11\ ln(10)\ \sigma_D^2)$ which is a truncated Jeffrey's prior for a scale parameter (Gelman et al. 2004) where $10^{-11} < \sigma_D^2 < 1$. This range was determined through preliminary ABC analysis. To simulate random values of D^*, we drew random values of θ and p^* as a proportion of θ which we denote as γ (where $\gamma = p^*/\theta$), from prior distributions. We then used the relationship $D^* = \theta(1-2\gamma)$ to find the random value of D^* to feed into the model.

Several empirical studies investigating the distribution of mutation effect size on expression indicate that the typical effect size is in the range 0.1% to 10% of expression (Metzger et al. 2015; Patwardhan et al. 2012; Melnikov et al. 2012). Since we scale expression units by $\sigma_m$this means that θ is likely greater than 4 σ_m. We therefore used a prior distribution for θ that is uniform between 4 and 10^3. For γ, we found from the data that the threshold must be less than 0.12 θ, and experimental data from several vertebrate cell types indicate that there are fewer than 10^4 mRNA transcripts of any given gene per cell (Mortazavi et al. 2008, Islam et al. 2010, Schwannhauser et al. 2011). We consider less than one transcript per cell as the loss of expression, which corresponds to a value of γ less than $1/10^4$. We conservatively set the prior for the log γ as a uniform distribution with $10^{-5} < \gamma < 0.12$.

Once random values for σ_D^2 and D^* were drawn from their prior distributions, evolution of D was simulated on the phylogenetic tree for the species taken from Betancur-R *et al.* (2013) (Figure 1). To discern the impact of ascertainment bias, we performed two analyses, one that excluded the electric fish and one that included them. The initial value at the root of the tree was

$D = 0$. We then proceeded through the tree from each node to its daughter nodes, with times between nodes specified by the tree. The value of D at a daughter node was determined by first asking if absorption had occurred at D^* or $-D^*$ using Equation 6. If absorption did not occur, then a random value of D between $-D^*$ and D^* was drawn from the conditional distribution for D using Equation 5. This process was repeated until the tips of the tree were reached. We then recorded which nodes (if any) had reached absorption and the values of D for those that had not.

The ABC rejection algorithm was implemented in two steps. First, the phylogenetic pattern of absorption was compared between the real data and each simulation. Simulations were rejected if the pattern of absorption on each of the two trees simulated did not match that of the two datasets (with and without the electric fish). In the second step, we used independent contrasts (IC) (Felsenstein 1985) to compare the remaining simulations to the data. The data from Thompson *et al.* (2014) is the expression ratio R = Scn4aa/Scn4ab, but D in the model is the expression difference. To compare those numbers, we used the equation

$$R = \frac{1+D/\theta}{1-D/\theta} \quad (1)$$

where θ is the optimal expression (see File S2). The independent contrasts of log R from the real data and each simulation were calculated at each node on the tree. We used the *pic* function in the R package *ape* to calculate vectors of IC. The Euclidean distance between the IC of each simulation and the real data was measured and used to reject > 99% of the remaining simulations. This threshold was determined by progressively narrowing the threshold of difference between simulation IC and data IC until convergence on a stable posterior distribution was achieved. We used the *abc* function in the R package *abc* to calculate the joint posterior distribution for the two parameters, σ_D^2, and D^* and local linear regression with an Epanechnikov kernel to correct for correlation between the statistic and each parameter value in the posterior distribution (Beaumont 2010). For the ABC analysis on the data containing the electric fish, 5 x 10^9 simulations were run with the electric fish and the posterior distribution contained 3135 simulations. For the data without the electric fish, 5 x 10^5 simulations were run with 322 simulations remaining in the posterior distribution.

References

Beaumont, M.A., 2010 Approximate Bayesian computation in evolution and ecology. Annu. Rev. Ecol. Evol. Syst. 41:379–406.

Betancur-R, R., R. E. Broughton, E. O. Wiley, K. Carpenter, J. A. Lo´pez, *et al.*, 2013 The tree of life and a new classification of bony fishes. PLoS Curr. 5: ecurrents.tol.53ba26640df0ccaee75bb165c8c26288.

Felsenstein, J. 1985 Phylogenies and the comparative method. Am. Nat. 125: 1-15.

Gelman, A., J. B. Carlin, H. S. Stern, D. B. Rubin, 2004 Bayesian data analysis, 2nd ed. Boca Raton (FL): Chapman & Hall/CRC.

Islam, S., U. Kjällquist, A. Moliner, P. Zajac, J.-B. Fan *et al.*, 2011 Characterization of the single-cell transcriptional landscape by highly multiplex RNA-seq. Genome Res. 21: 1160–1167.

Melnikov, A., A. Murugan, X. Zhang, T. Tesileanu, L. Wang *et al.*, 2012 Systematic dissection and optimization of inducible enhancers in human cells using a massively parallel reporter assay. Nat. Biotechnol. 30: 271–277.

Metzger, B. P. H., D. C. Yuan, J. D. Gruber, F. Duveau, and P. J. Wittkopp, 2015 Selection on noise constrains variation in a eukaryotic promoter. Nature 521: 344–347.

Mortazavi, A., B. A. Williams, K. McCue, L. Schaeffer, and B. Wold, 2008 Mapping and quantifying mammalian transcriptomes by RNA-Seq. Nat. Methods 5: 621–628.

Patwardhan, R. P., J. B. Hiatt, D. M. Witten, M. J. Kim, R. P. Smith *et al.*, 2012 Massively parallel functional dissection of mammalian enhancers in vivo. Nat. Biotechnol. 30: 265–270.

Schwanhäusser, B., D. Busse, N. Li, G. Dittmar, J. Schuchhardt *et al.*, 2011 Global quantification of mammalian gene expression control. Nature 473: 337–342.

Thompson, A., D. Vo, C. Comfort, H. H. Zakon, 2014 Expression evolution facilitated the convergent neofunctionalization of a sodium channel gene. Mol. Biol. Evol. 31(8): 1941-1955.